LEVEL II

AD A080025

DYNAMICS RESEARCH CORPORATION

(18) (19)
Report No. NADC-76097-30-Vol-I
(14) R-3033U; 1273-Vol-I (12)

(6)
APPLICATION OF THE ESTIMATION-BEFORE-MODELING (EBM) SYSTEM IDENTIFICATION METHOD TO THE HIGH ANGLE OF ATTACK/SIDESLIP FLIGHT OF THE T-2C JET TRAINER AIRCRAFT.

Volume I • Executive Summary •

(11) 12 November 1979

(12) 60 (9) Final rept.,

Prepared for:

Naval Air Development Center
Warminster, Pennsylvania 18974

(15) Contract No.: N62269-76-C-0342

(10) Harold L. /Stalford

Prepared by:

Dynamics Research Corporation
Systems Division
60 Concord Street
Wilmington, Massachusetts 01887

Approved for Public Release: Distribution Unlimited

Unclassified

SECURITY CLASSIFICATION OF THIS PAGE (When Data Entered)

REPORT DOCUMENTATION PAGE		READ INSTRUCTIONS BEFORE COMPLETING FORM
1. REPORT NUMBER NADC-76097-30	2. GOVT ACCESSION NO.	3. RECIPIENT'S CATALOG NUMBER
4. TITLE (and Subtitle) Application of the Estimation-Before-Modeling (EBM) System Identification Method to High Angle-of-Attack/Sideslip Flight of the T-2C Jet Trainer Aircraft. Vol. I - Executive Summary		5. TYPE OF REPORT & PERIOD COVERED Final Report 6. PERFORMING ORG. REPORT NUMBER 1273
7. AUTHOR(s) Harold L. Stalford		8. CONTRACT OR GRANT NUMBER(s) N62269-76-C-0342
9. PERFORMING ORGANIZATION NAME AND ADDRESS Dynamics Research Corporation 60 Concord Street Wilmington, Massachusetts 01887		10. PROGRAM ELEMENT, PROJECT, TASK AREA & WORK UNIT NUMBERS
11. CONTROLLING OFFICE NAME AND ADDRESS Naval Air Development Center (Code 6053) Warminster, Pennsylvania 18974		12. REPORT DATE 12 November 1979 13. NUMBER OF PAGES
14. MONITORING AGENCY NAME & ADDRESS (if different from Controlling Office)		15. SECURITY CLASS. (of this report) Unclassified 15a. DECLASSIFICATION/DOWNGRADING SCHEDULE

16. DISTRIBUTION STATEMENT (of this Report)

Approved for Public Release; Distribution Unlimited

17. DISTRIBUTION STATEMENT (of the abstract entered in Block 20, if different from Report)

18. SUPPLEMENTARY NOTES

19. KEY WORDS (Continue on reverse side if necessary and identify by block number)

System Identification	Aircraft	EBM
Aerodynamic Derivatives	T-2C	
Estimation	High Alpha	
Modeling	High Beta	

20. ABSTRACT (Continue on reverse side if necessary and identify by block number)

This report (Volume I) summarizes the development and application of the "Estimation-Before-Modeling (EBM) method for aircraft parameter identification in the non-linear flight regime. The method utilizes a "two-step" approach wherein model independent states, forces and moments are first estimated and then state and control dependent model parameters are obtained using a Stepwise →next page

DD FORM 1 JAN 73 1473 EDITION OF 1 NOV 65 IS OBSOLETE

Unclassified

SECURITY CLASSIFICATION OF THIS PAGE (When Data Entered)

cont.

Multiple Linear Regression (SLMR) approach. In the second step (SLMR) the angle of attack and sideslip and control input space for all available flight data is divided into small subspaces and force and moment coefficients are modeled within each subspace.

The method is applied to both simulated and actual flight data for a T-2C jet trainer aircraft in the stall and post-stall flight regimes.

Volumes II and III of this report present detailed descriptions of the EBM method and its application.

FOREWORD

The work described in the report was sponsored by the Flight Dynamics Branch of the Air Vehicle Technology Department of the Naval Air Development Center. Mr. Robert L. Fortenbaugh, Mr. A. Piranian, Mr. Ronald L. Nave and Mr. John Clark served as the Navy Technical Monitors for the Naval Air Development Center. Mr. Carmen J. Mazza was NADC program manager.

The project was managed by Dr. Harold Stalford. This report is a summary of the simulation study documented in Volume II and a summary of the real flight test data analysis documented in Volume III.

TABLE OF CONTENTS

LIST OF FIGURES

LIST OF FIGURES (Cont'd)

LIST OF FIGURES (Cont'd)

LIST OF FIGURES

LIST OF TABLES

1. INTRODUCTION

This study was motivated by the inability of empirical and theoretical techniques to accurately predict the nonlinear aerodynamics of the high angle of attack/sideslip domain for aircraft. The Naval Air Development Center (NADC) took the direction to extract the nonlinear aerodynamics from actual flight test data using system identification and modeling techniques. Success in this direction allows predicted effects to be correlated with the actual effects to determine the scaling, trending, reformulation, etc. that must be applied to the prediction to match the actual. By performing this correlation for several existing aircraft it will build confidence in the designer's ability to predict the performance and stability and control characteristics of proposed aircraft.

The T-2C is a light jet trainer aircraft which was instrumented and operated by NADC for the express purpose of producing high angle of attack flight data. The data along with a wind tunnel model of the T-2C was supplied to Dynamics Research Corporation (DRC) for processing with an advanced system identification method called the Estimation-Before-Modeling (EBM) technique. The desired results of applying the EBM technique to flight data are (1) optimal, smoothed, time history estimates of the vehicle state parameters and (2) state-dependent models for the coefficients of the forces and moments acting on the vehicle.

The scope of this aircraft system identification study is confined 1) to processing 16 maneuvers of synthetic T-2C flight test data, which generated using the T-2C wind tunnel model and a theoretical prediction model, and 2) to processing 18 maneuvers of actual T-2C flight test data.

The objective of the study is two-fold:

1. Develop and refine the EBM method for application to the identification of aircraft aerodynamic characteristics in the non-linear (high angle of attack/sideslip) flight regime.

2. Apply the EBM method to both simulated and actual flight test data for a T-2C jet trainer aircraft at high angles of attack and sideslip.

A major contribution of this study is the approach taken to identify, from actual flight test data in high angle of attack/sideslip flight regimes, the highly nonlinear aerodynamic stability and control characteristics. The EBM technique is a two-step approach to the identification of aircraft aerodynamics (See Figure 1-1). The first step which is the nonlinear estimation part uses Gauss-Markov processes to model the accelerations due to aerodynamic forces, (e.g., drag, sideslip and lift) and moments (e.g., roll, pitch and yaw). It employs an extended Kalman-Bucy filter/ Bryson-Frazier smoother to generate smoothed estimates of the states, aerodynamic forces and moments time histories, and measurement biases and scale factors. In the second step which is the modeling part, the Stepwise Multiple Linear Regression (SMLR) method is used together with the subspace modeling to identify the nonlinear dependency of the aerodynamic coefficients on aircraft states and controls.

Any system identification method must perform both estimation and modeling. A unique feature of the EBM technique is the separation of the estimation of the aircraft states (i.e., the first step) from the modeling of the aerodynamics coefficients (i.e., the second step). It is this separation that gives the EBM technique its power as a modeling tool. It decouples the highly complex modeling problem into six simpler ones. Instead of the problem of modeling all six coefficients simultaneously, each coefficient is modeled independently of the others. In addition,

OVERVIEW OF EBM METHOD

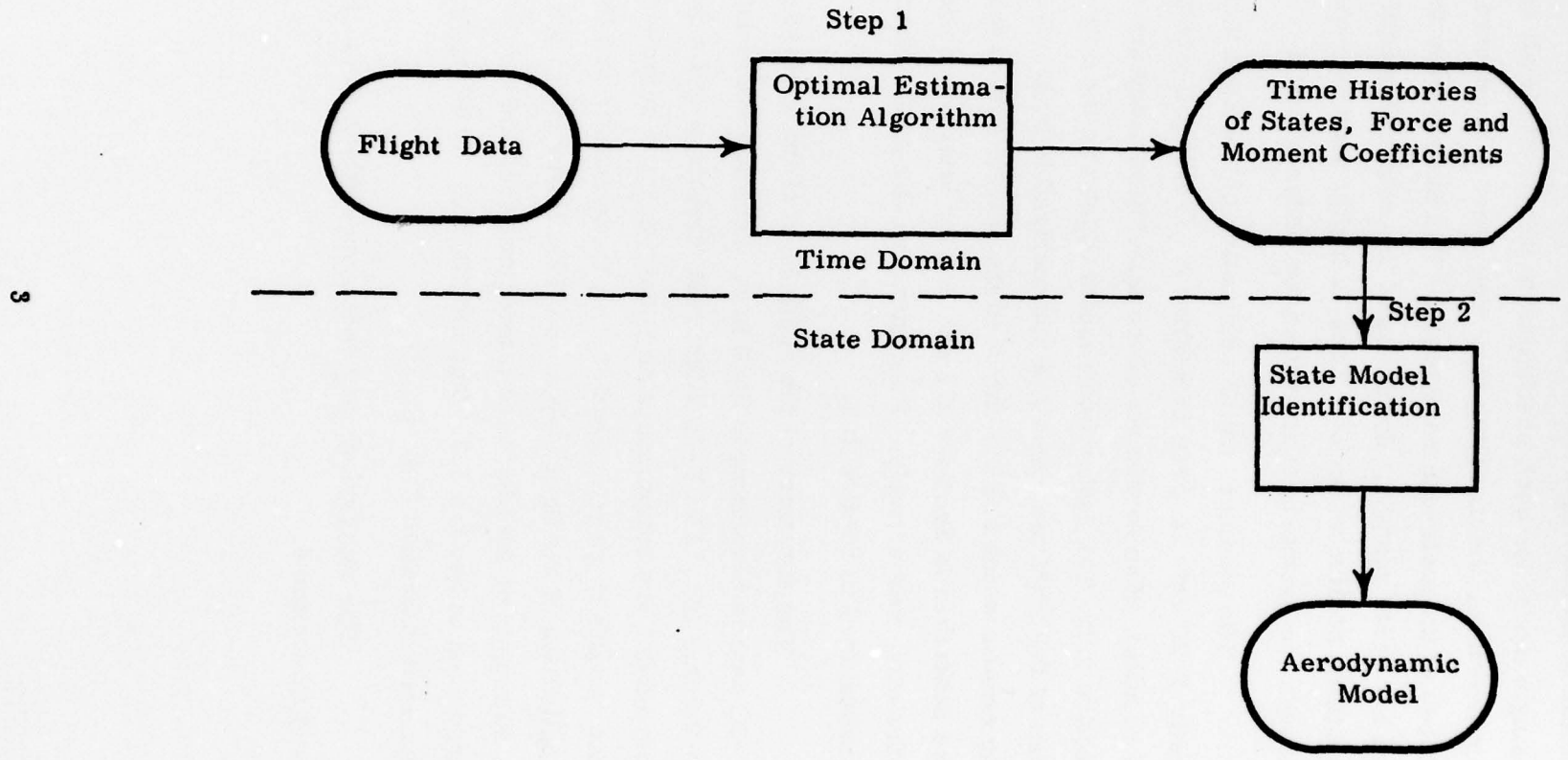

instead of identifying a model of each coefficient for each maneuver, a single model for each coefficient is identified for all maneuvers. Furthermore, the modeling of a coefficient is conducted over subspaces of the state-control domain. The models over the subspaces are low order models. Synthesis of the subspace models provides the identified nonlinear model. Thus, a highly nonlinear model is identified through the synthesis of identified low order models.

The summary of the application of the EBM technique to synthetic T-2C data is given in Section 2. (Volume II contains the full set of results). The conditions of the simulation study are described in Section 2.1. The estimation results which are the output of the first step of the EBM technique are summarized in Section 2.2. The modeling results which are the output of the second step of the EBM technique are described in Sections 2.3 and 2.4 for lateral and longitudinal coefficients, respectively. Prediction results of the identified model are summarized in Section 2.5.

The summary of the application of the EBM technique to real T-2C data is presented in Section 3. (The full set of results are given in Volume III). The T-2C flight test conditions and a description of the maneuvers are summarized in Section 3.1. A summary of the estimation results is given in Section 3.2; these results are the output of the application of the first step of the EBM technique to the real T-2C data. A summary of the identified lateral model of the actual T-2C aircraft is presented in Section 3.3. The longitudinal modeling results are summarized in Section 3.4.

The conclusions and recommendations of the study are summarized in Section 4.

2. SUMMARY OF SIMULATION STUDY RESULTS

2.1 CONDITIONS OF THE SIMULATION STUDY

A T-2C wind tunnel data model and a theoretical prediction model of the dynamic derivatives, all supplied by NADC, formed the 6 DOF model used in the simulation study to generate synthetic test flight data. The synthetic maneuvers were made as realistic as possible by using the control input time histories of the actual T-2C test flight data. Sixteen maneuvers of available T-2C actual flight test data were used to provide the control time histories and the initial conditions for generating sixteen synthetic maneuvers. These are summarized in Table 2.1-1. The designation SF1M1 in the first column denotes that the controls are from maneuver 1 of flight 1 of the actual flight test data. The type of control is described in the third column for each maneuver. Some characteristics of the synthetic maneuvers are given in the last column.

Under the conditions described above, the equations of motion were integrated while exciting the synthetic T-2C model with the control inputs from the actual flight test data. When this was done, it was found that a few maneuvers diverged after a few seconds, and the responses for most maneuvers were totally different from the actual flight test data. The synthetic model exhibited frequencies and amplitudes that were very much higher than the actual flight test data. An example of this behavior is shown in Figure 2.1 of Volume II. In that example, the actual aircraft motion had a maximum angle of attack of 25°, but the synthetic maneuver had an angle of attack as high as 60°. The problem was found to be in the theoretical prediction model of C_{n_p}. By trial and error, the constant value of -.06 for C_{n_p} was found to give stability to the simulated data and to provide synthetic maneuvers which agreed better with the actual flight

Table 2.1-1 Description of the Synthetic T-2C Data Processed with the EBM System Identification Method

Synthetic Flight No. and Maneuver No.	Approximate Duration of Maneuver (sec.)	Type of Input	Comments
SF1M1	16	Aft Stick, full rudder pedal	Roll departure
SF2M1	34	Random fore & aft stick	α (max) = 30°
SF2M2	35	Random side to side lateral stick	Low α
SF2M3	45	Sequential doublets - δ_e, δ_a, δ_r	High angular rates
SF3M1	35	Longitudinal Doublet	α (max) = 25°
SF3M2	26	Random Side to Side Rudder Input	Low α
SF3M3	29	Sequential Random - δ_e, δ_a, δ_r ($\beta_o = 0^o$)	α (max) = 20°
SF4M1	21	Longitudinal Stick ramp plus sine wave	α (max) = 30°
SF4M2	74	Sequential Random - δ_e, δ_a, δ_r ($\beta_o = -5^o$)	Roll departure
SF4M3	49	Sequential Random - δ_e, δ_a, δ_r ($\beta_o = 5^o$)	High roll rate
SF4M5	60	Longitudinal Limit Cycle	α (max) = 25°
SF4M6	38	Shallow Bank to Stall	α (max) = 30°
SF4M7	45	Steep Bank to Stall	α (max) = 34°
SF4M8	41	Pull-up from Dive	α (max) = 29°
SF4M9	28	Coordinated Control Spin Entry	α (max) = 40°
SF4M10	27	Coordinated Control Spin Entry	α (max) = 46°

test data. Fixing the value of C_{n_p} was no loss to checking out the EBM technique since there was a gain in stability and since other dynamic derivatives C_{ℓ_p}, C_{ℓ_r}, and C_{n_r} provided similar non-linearities as exhibited in the original model of C_{n_p}.

2.2 ESTIMATION RESULTS - FIRST STEP OF THE EBM METHOD

The time history of the states for each of the sixteen synthetic maneuvers were fed into NADC supplied measurement equations to produce noise-free measurements. The measurements were corrupted with white, zero-mean gaussian noise having the standard deviations supplied by NADC. These standard deviations are shown in Table 2.2-1 under the heading "Measurement Noise Level" for each measured variable. The corrupted measurements were processed using an extended Kalman-Bucy filter/Bryson-Frazier smoother to obtain estimated values of the states and of the forces and moments. For the purpose of checking the performance of the filter/smoother, the estimated values were fed into the measurement equations and the RMS values of the difference between these "smoothed" measurement values and the noise-free measurements were computed. The RMS values averaged for all sixteen maneuvers are presented in the last column of Table 2.2-1. This table shows how much of the measurement error was taken out by the estimation process. The amount of noise corrupting the synthetic data is given in the fourth column. The amount of noise remaining after the estimation process is shown in the last column. For example, the noise level on the angle of attack is reduced by the estimation process from .0028 rad to .0005 rad, which is a reduction of 82% so that only 18% of the original noise remains in the smoothed data. Noise levels are reduced by at least 50% for most of the other measured variables as well. Using Table 2.2-1 we make the following observations of the estimation results. The estimation process has reduced the error level from .24 to .12 for the acceleration measurement A X NOSE in the x-direction. The errors on the

Table 2.2-1 Comparison Between Measurement Noise and Estimation Error Levels Taken Over all Sixteen Maneuvers

Measured	Descriptive Name	Units	Measurement Noise Level (1σ)	RMS Value of Estimation Error
Z_1	A X NOSE	m/sec^2	.24	.12
Z_2	A Z C G	m/sec^2	1.05	.23
Z_3	A Z NOSE	m/sec^2	1.05	.26
Z_4	A Z TAIL	m/sec^2	1.05	.26
Z_5	A Z R	m/sec^2	1.05	.30
Z_6	A Z L	m/sec^2	1.05	.31
Z_7	A Y C G	m/sec^2	.24	.07
Z_8	A Y NOSE	m/sec^2	.24	.08
Z_9	A Y TAIL	m/sec^2	.24	.08
Z_{10}	THETA	rad	.00087	.0006
Z_{11}	PHI	rad	.00087	.0003
Z_{12}	Roll Rate	rad/sec	.0017	.0013
Z_{13}	Pitch Rate	rad/sec	.0017	.0011
Z_{14}	Yaw Rate	rad/sec	.0017	.0008
Z_{15}	Altitude	m	10.	1.5
Z_{16}	Air Speed	m/sec	.43	.06
Z_{17}	ALPHA	rad	.0028	.0005
Z_{18}	BETA	rad	.0028	.0004

acceleration measurements in the z-direction (i.e., AZCG, ..., AZL) have been reduced by a factor of 3 or 4. The errors on the acceleration measurement in the y-direction have been reduced by a factor of 3. The errors on θ and ϕ have been reduced by a factor of 3. The errors on the roll, pitch and yaw rates have been reduced by less than a factor of 2. The errors on air speed are less by a factor of 7. The errors on α and β have been cut down by a factor of 5 or 6. These estimation results demonstrate that the Kalman-Bucy filter/Bryson-Frazier smoother performs well as a nonlinear estimator of aircraft states, forces and moments.

2.3 LONGITUDINAL MODEL IDENTIFICATION RESULTS - SECOND STEP OF THE EBM TECHNIQUE

The smooth data provided by the estimation process is first analyzed for its distribution in the α, β state space. The distribution of the smooth data for the δ_e range [-15°, -10°] is shown in Table 2.3-1. Each number in a subspace is the number of times that the sixteen maneuvers had data points on the subspace. About fifteen data points are needed to model the longitudinal coefficients on a subspace. The twenty-five subspaces containing at least fifteen points are enclosed with a heavy black line.

Other subdivisions were made in the δ_e space to define the final set of subspaces for modeling. That is, the longitudinal coefficients were modeled on subspaces defined by α, β and δ_e. The subspaces are described in Table 2.3-2. The number of subspaces are presented in the last column for the corresponding δ_e and β intervals. From the table we see that the α, β and δ_e modeling space is subdivided into 88 subspaces to be modeled with the SMLR technique. Instead of trying to match the entire data with one equation containing a very large number of terms, we have divided the data from the 16 maneuvers into 88 groups

Table 2.3-1 Density of Modeling Data for the Subspaces Contained in the Region Defined by $|\beta| = 0°$ to $30°$ and $\alpha = -4°$ to $35°$ and by δ_e min = -15° and δ_e max = -10°

End points of subspaces for α	End points of subspaces for $\|\beta\|$							
	0°	2°	5°	10°	15°	20°	25°	30°
-4°	2	2	0	0	0	0	0	
0°	15	4	1	0	0	0	0	
4°	31	2	1	4	0	0	0	
8°	82	27	6	4	0	0	0	
12°	101	54	6	0	0	0	0	
14°	64	-23	22	0	0	1	0	
15°	54	19	32	1	1	2	0	
16°	144	43	35	13	2	0	0	
18°	109	32	33	11	3	0	0	
20°	99	66	53	28	12	0	0	
25°	16	21	17	6	0	0	0	
30°	0	0	1	0	0	0	0	
35°								

such that we can model each region with a simple low-order model. Then the resulting 88 low-order models are combined into a global non-linear model.

From Table 2.3-2 we observe that the subspaces containing enough data for modeling do not form a covering of the entire α, β, δ_e space and there are holes (e.g. third, fourth and fifth rows of the table). We see that the controls used were inadequate to generate data in several regions, especially at high β and also for the combination of low α and high δ_e. There are not enough data points for α beyond 35°.

Table 2.3-2 Data Distribution for Longitudinal Modeling

$\delta_{e_{min}}$ (deg)	$\delta_{e_{max}}$ (deg)	β min (deg)	β max (deg)	α min (deg)	α max (deg)	No. of Subspaces
-10	0	0	2	-4	25	10
		2	5	0	25	9
		5	10	4	14	3
		5	10	16	18	1
		5	10	20	25	1
		10	15	8	12	1
-15	-10	0	2	0	30	10
		2	5	8	30	8
		5	10	14	30	6
-17	-13	10	15	20	25	1
-25	-15	0	2	8	35	9
		2	5	12	35	8
		5	10	12	14	1
		5	10	16	30	4
-25	-30	0	2	14	35	7
		2	5	16	35	5
		5	10	18	35	4

Identification of C_x, C_z and C_m using the SMLR technique was performed in all subspaces and then synthesized into a global model. The global model is documented in Section 4.3 and 4.4 of Volume II. Models of C_x, C_z and C_m and their derivatives with respect to α, β and δ_e were identified for $0^\circ \leq \alpha \leq 35^\circ$, $0^\circ \leq |\beta| \leq 10^\circ$, and $-24^\circ \leq \delta_e \leq 0^\circ$. The dynamic derivatives $C_{z_q} + C_{z_{\dot{\alpha}}}$ and $C_{m_q} + C_{m_{\dot{\alpha}}}$ were identified for $0 \leq \alpha \leq 35^\circ$. Examples of comparisons between the identified models and the synthetic model (i.e., wind tunnel and theoretical prediction) are given in Figures 2.3-1, 2.3-2, 2.3-3 and 2.3-4. For $\delta_e = -25^\circ$ and $|\beta| = 5^\circ$ the identified model of $C_x(\alpha)$, $0^\circ \leq \alpha \leq 35^\circ$, is compared with the wind tunnel model in Figure 2.3-1. The wind tunnel values are represented by a "square" symbol and the identified values are denoted by a "triangular" symbol. The identified values lie almost on top of the wind tunnel values.

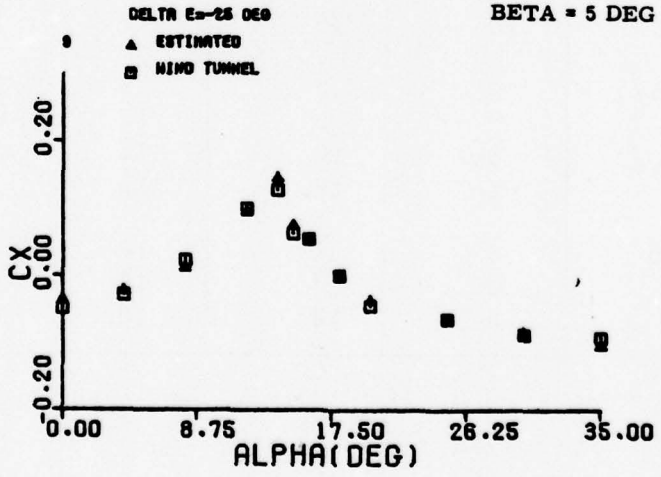

Figure 2.3-1 Comparison between the identified model of the C_x coefficient and the T-2C wind tunnel model for $\beta = 5^\circ$ and $\delta_e = -25^\circ$: Synthetic data

For $\delta_e = -15^\circ$ and $|\beta| = 10^\circ$ the identified model of $C_z(\alpha)$, $0^\circ \le \alpha \le 35^\circ$, is compared with the wind tunnel data in Figure 2.3-2. All identified values are highly accurate except for $\alpha = 30^\circ$. We see from Table 2.3-1 that almost no data points were available for modeling in the neighborhood of $\alpha = 30^\circ$, $|\beta| = 10^\circ$, and $\delta_e = -15^\circ$. Yet, the identified value at $\alpha = 30^\circ$ is close to the wind tunnel value.

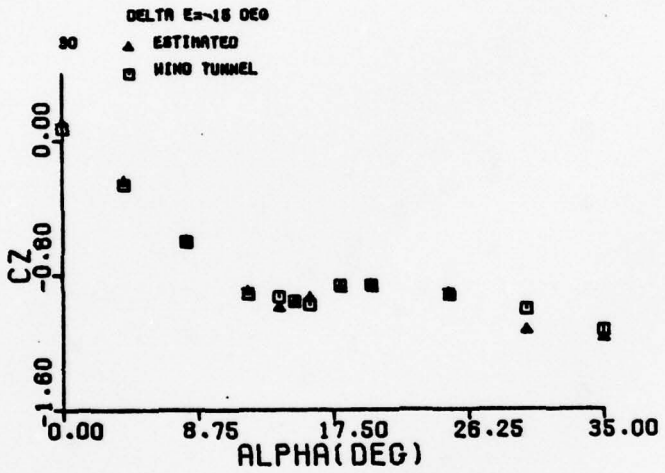

Figure 2.3-2 Comparison between the identified model of the C_z coefficient and the T-2C wind tunnel data for $\beta = 10^\circ$ and $\delta_e = -15^\circ$: Synthetic data

For $|\beta| = 5^\circ$, the identified model of $C_m(\alpha)$, $0^\circ \le \alpha \le 35^\circ$, $\delta_e = -25^\circ$, -15°, -10°, 0°, is compared with the wind tunnel data in Figure 2.3-3. The four curves represented in the figure correspond to $\delta_e = -25^\circ$, -15°, -10° and 0°. Observe how the two wind tunnel data curves with $\delta_e = -15^\circ$ and -25° coincide at low α but differ considerably at high α. This nonlinear separation in the wind tunnel model was accurately identified.

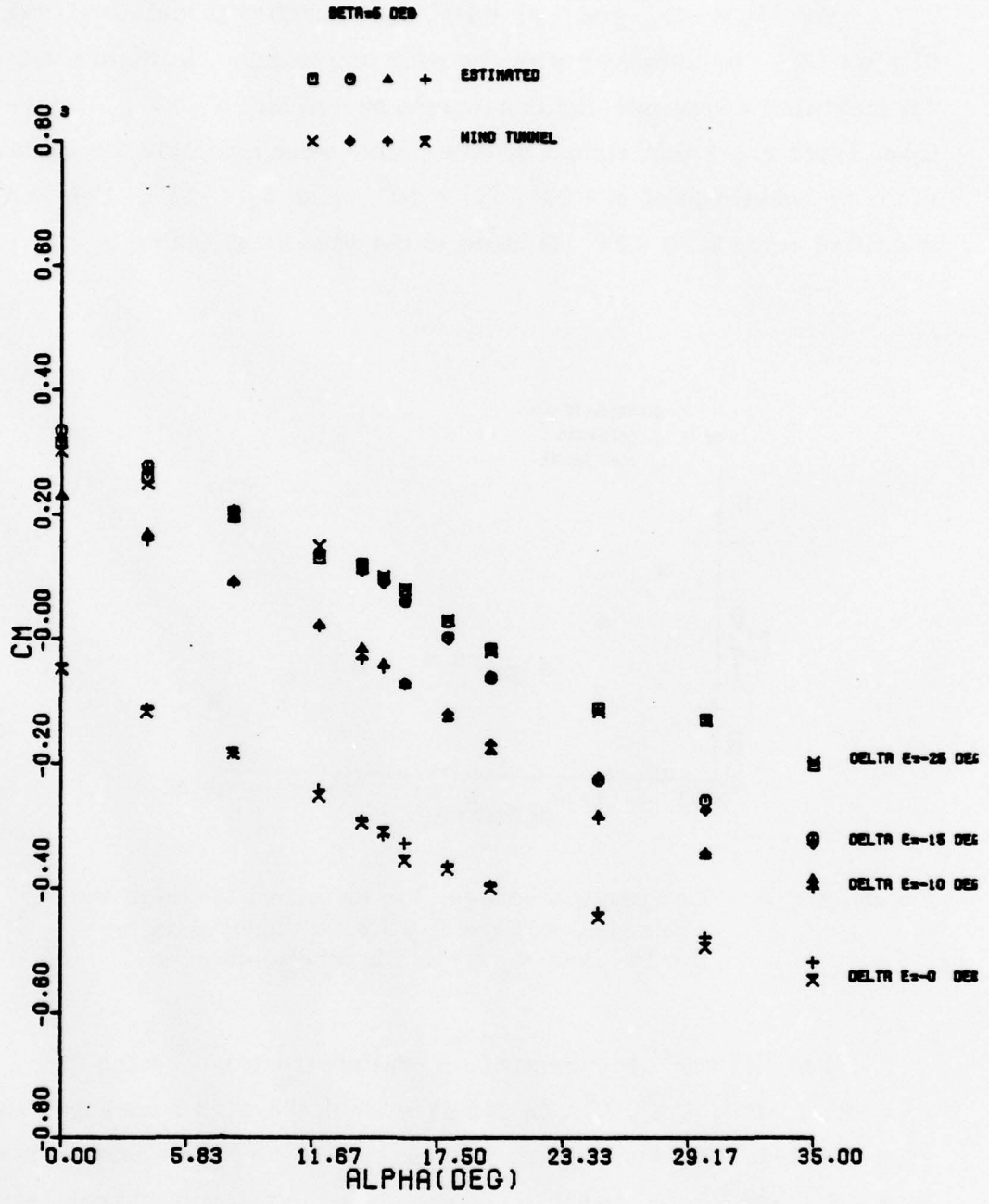

Figure 2.3-3 Comparison between the identified model of the C_m coefficient and the T-2C wind tunnel data for $\beta = 5^o$ and $\delta_e = -25^o$, -15^o, -10^o and 0^o: Synthetic data

The identified model of $C_{m_q}(\alpha) + C_{m_{\dot{\alpha}}}(\alpha)$, $0^\circ \leq \alpha \leq 35^\circ$ is compared in Figure 2.3-4 with the theoretical prediction model of $C_{m_q} + C_{m_{\dot{\alpha}}}$. We have once again excellent agreement between the identified model that came out of the simulation study and the synthetic model that went into it.

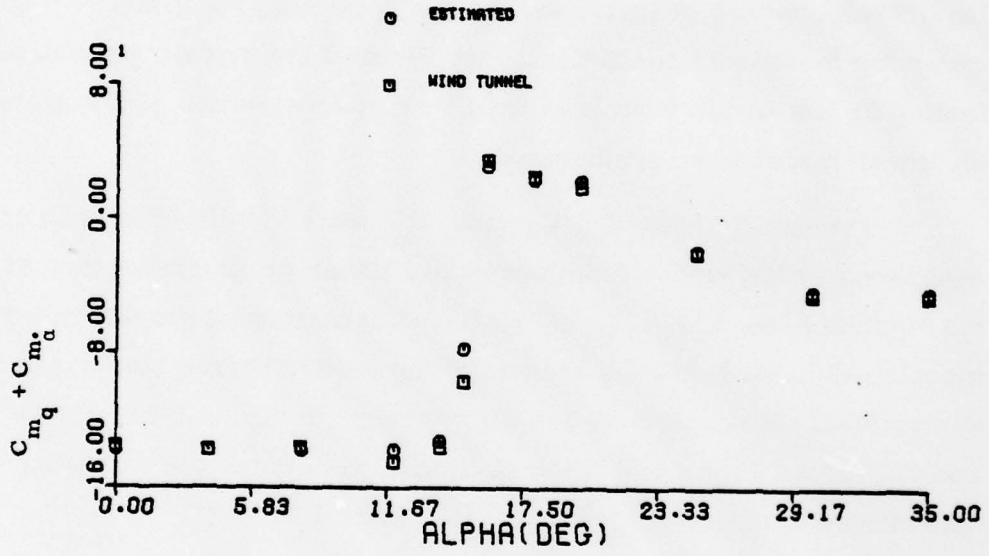

Figure 2.3-4 Comparison between the identified model of the combined derivatives $C_{m_q} + C_{m_{\dot{\alpha}}}$ and the theoretical prediction model: Synthetic data

The results presented in Figures 2.3-1, 2.3-2, 2.3-3, 2.3-4 are typical of the identified models for C_x, C_z and C_m obtained in the simulation study.

2.4 LATERAL MODEL IDENTIFICATION RESULTS - SECOND STEP OF THE EBM TECHNIQUE

The α and β spaces were used to define the subspaces for lateral modeling. The α-space was divided into 18 intervals and the β space was partitioned into 3 intervals: 0°-2°, 2°-5°, and 5°-10°. This partitioning on α and β produced 54 subspaces. There was enough data with $20^\circ \leq \alpha \leq 25^\circ$ and $10^\circ \leq |\beta| \leq 15^\circ$ to provide an additional subspace, making a total of 55 subspaces for lateral modeling. Thus, instead of trying to find one very complex model of high order for the lateral coefficients, we reduced the modeling problem to finding 55 low-order models in the 55 subspaces, which give a global nonlinear model when synthesized.

The coefficients C_y, C_ℓ and C_n were identified in each of the subspaces as low-order functions (i.e., linear or quadratic terms) of the variables α, β, δ_e, δ_r, p, r and $\dot{\beta}$. Synthesizing the identified models produced nonlinear models of the static, control and dynamic derivatives. In particular, for the range of α and β with $0 \leq \alpha \leq 30^\circ$ and $0 \leq |\beta| \leq 10^\circ$ we identified nonlinear models for the following derivatives of the coefficients C_y, C_ℓ and C_n:

C_y	C_ℓ	C_n
$C_{y_\beta}(\alpha, \beta)$	$C_{\ell_\beta}(\alpha, \beta)$	$C_{n_\beta}(\alpha, \beta)$
$C_{y_{\delta_r}}(\alpha, \beta)$	$C_{\ell_{\delta_r}}(\alpha, \beta)$	$C_{n_{\delta_r}}(\alpha, \beta)$
$C_{y_{\delta_a}}(\alpha, \beta)$	$C_{\ell_{\delta_a}}(\alpha, \beta)$	$C_{n_{\delta_a}}(\alpha, \beta)$

For the α-range $0 \leq \alpha \leq 30^\circ$ we identified nonlinear models (except for C_{n_p} which is a constant) for the following dynamic derivatives of the coefficients C_y, C_ℓ and C_n:

C_y	C_ℓ	C_n
$C_{y_r}(\alpha)$	$C_{\ell_r}(\alpha)$	$C_{n_r}(\alpha)$
	$C_{\ell_p}(\alpha)$	$C_{n_p}(\alpha)$
	$C_{\ell_\alpha}(\alpha, \beta)$	$C_{n_\alpha}(\alpha, \beta)$
	$C_{\ell_{r\alpha}}(\alpha, \beta)$	$C_{n_{r\alpha}}(\alpha, \beta)$
	$C_{\ell_{p\alpha}}(\alpha, \beta)$	

The identification process was successful in separating C_{n_r} and $C_{n_{\dot\beta}}$, in separating C_{ℓ_r} and $C_{\ell_{\dot\beta}}$ and in correctly determining that the derivatives $C_{\ell_{\dot\beta}}$ and $C_{n_{\dot\beta}}$ are insignificant. (The synthetic model values for these two derivatives are zero).

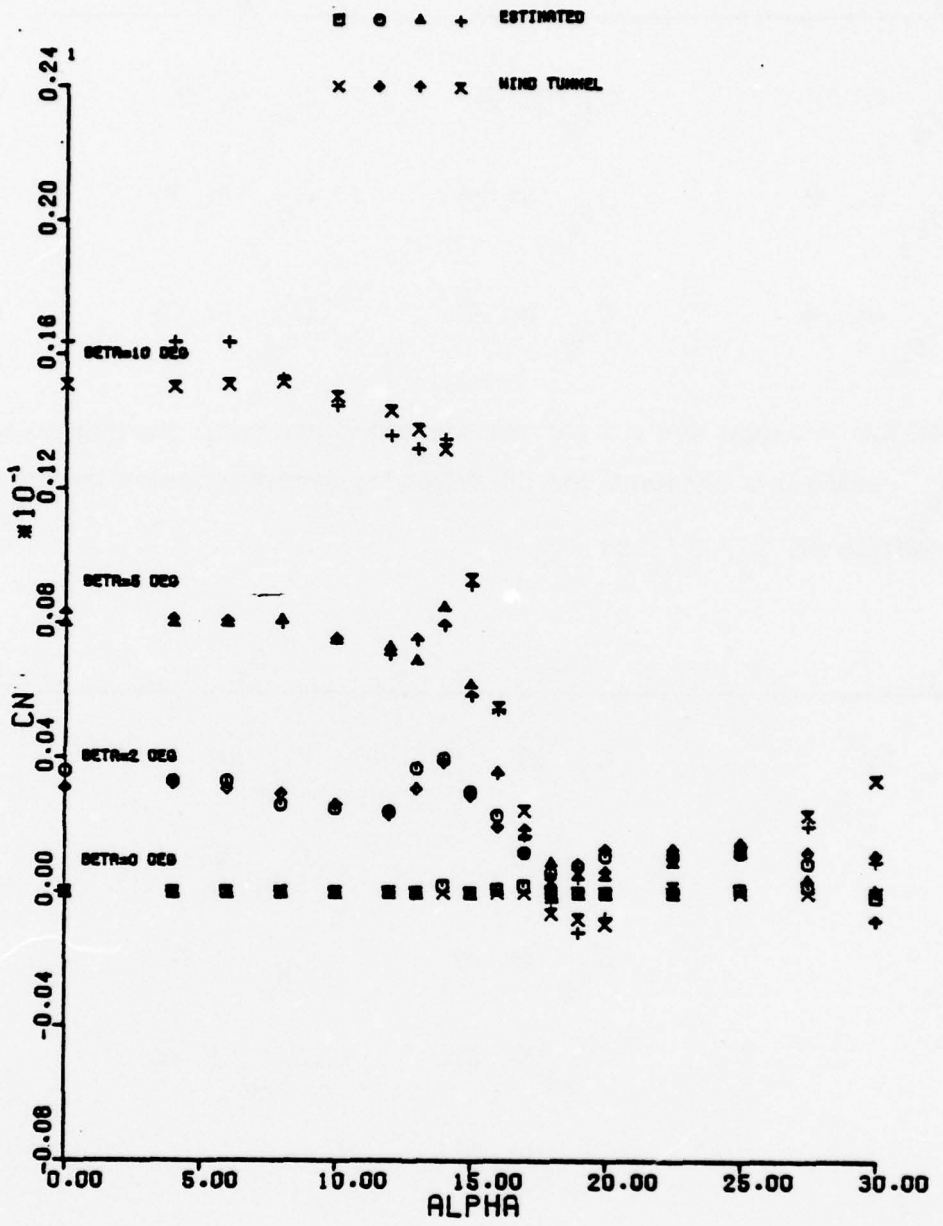

Figure 2.4-1 Comparison between the identified model of the C_n coefficient and the T-2C wind tunnel data for $\beta = 0^o$, 2^o, 5^o and 10^o: Simulation Study

Some typical examples of the identified models are shown in Figures 2.4-1, 2.4-2, 2.4-3 and 2.4-4. The identified model of $C_n(\alpha, \beta)$ for $\beta = 0^o$, 2^0, 5^o and 10^o is compared with the wind tunnel data values in Figure 2.4-1. For $\beta = 2^o$ and $\beta = 5^o$, C_n initially decreases in magnitude with α, increases near stall (i.e., $\alpha = 15^o$), decreases rapidly after stall becoming nearly zero at $\alpha = 20^o$ and then remains very small in magnitude. For $\beta = 10^o$, C_n decreases in magnitude with α, falls sharply in the stall region and dips to a negative value at $\alpha = 18^o$. With further increase in α, the value of C_n increases slightly. Very good agreement is indicated between the identified model and the wind tunnel model. The high nonlinearities present around the stall region were accurately identified.

We see in Figure 2.4-2 that the identification process obtained good estimates of $C_{n_\beta}(\alpha, \beta)$ at $\beta = 2^o$. It is positive at low α, declines in value rapidly through stall and becomes extremely small or negative in the post stall region.

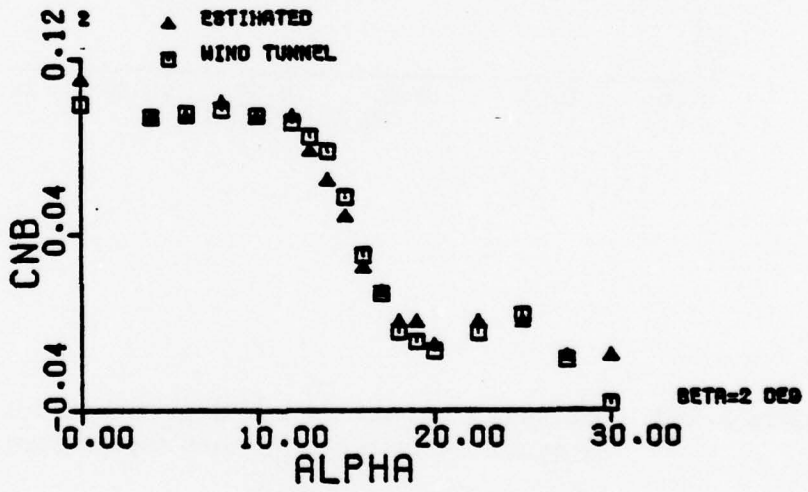

Figure 2.4-2 Comparison between the identified model of the derivative C_{n_β} and the T-2C wind tunnel data for $\beta = 2^o$: Simulation Study

In Figure 2.4-3 we see that the identified values of the dynamic derivative C_{n_p} is nearly a constant value of -.06 which is the synthetic model value used in this simulation study.

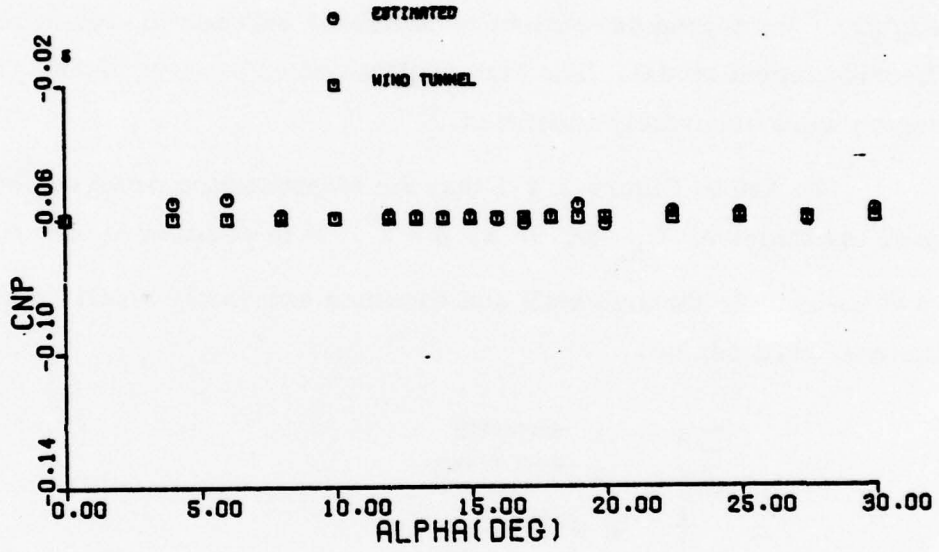

Figure 2.4-3 Comparison between the identified model of the dynamic derivative C_{n_p} and the synthetic model of C_{n_p} : Simulation Study

In Figure 2.4-4 we observe the comparison between the identified model for C_{ℓ_p} and the theoretical prediction model used in this simulation study. The roll damping derivative C_{ℓ_p} stays constant up to an

angle of attack of 10^{o} when it starts decreasing. Immediately after stall it jumps to an unstable value of 0.3 and stays positive up to an α of 20^{o}. Beyond that the roll damping is very small. The identified model follows this highly nonlinear variation extremely well.

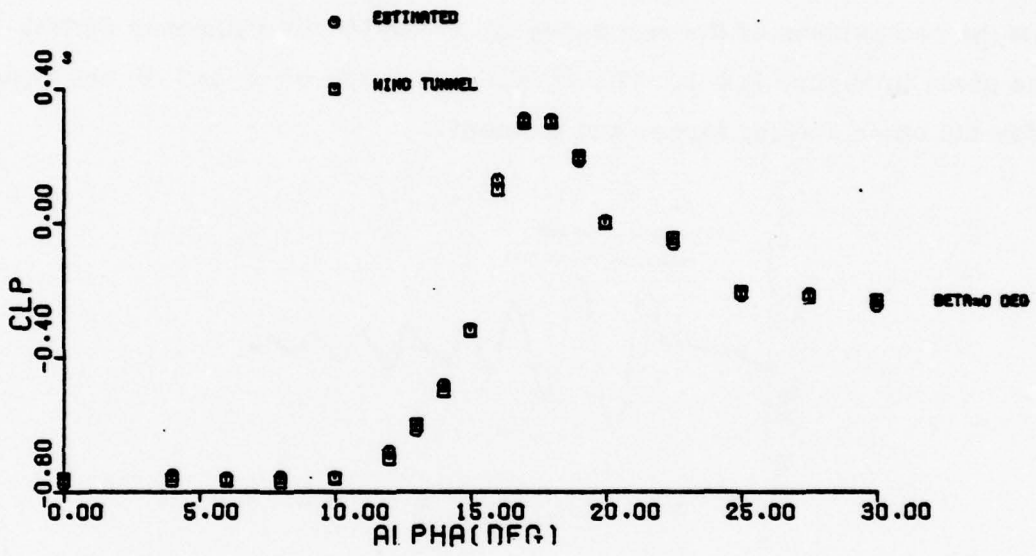

Figure 2.4-4 Comparison between the identified model of the dynamic derivative C_{ℓ_p} and the theoretical prediction model: Simulation Study

2.5 PREDICTION RESULTS

The identified global model of the six coefficients C_x, C_y, C_z, C_ℓ, C_m and C_n was assessed as to how well the identified model predicts (1) the sixteen maneuvers used in the identification and (2) a maneuver not used in the identification process.

For the first case, excellent agreement between the original synthetic (i.e., "true") response and the response predicted by the identified model was obtained for most of the maneuvers. An example of the comparison of the responses of α and β for maneuver SF2M3 is given in Figure 2.5-1. The excellent matches of α and β are typical for the other states, forces and moments.

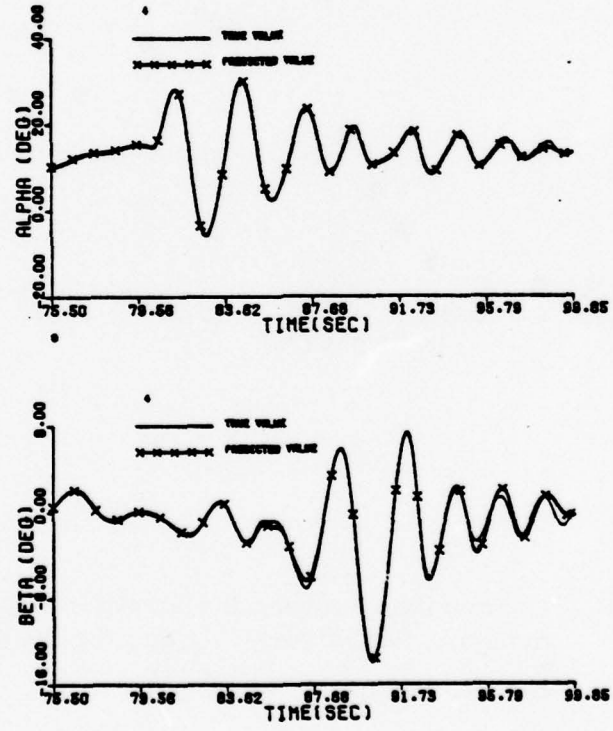

Figure 2.5-1 Comparison between the predicted and the true time histories of α and β for SF2M3

For some maneuvers the response of the identified model went into regions where no models were identified. Extrapolating the identified model into these regions led to a response that was sometimes different from the "true" response.

For the second case, new control inputs (Figure 2.5-2) were chosen to excite both the identified model and the synthetic model. Sinusoidal inputs were used. The responses of α and β are compared in Figure 2.5-3. We notice that the response predicted by the identified model and the actual response are in good agreement.

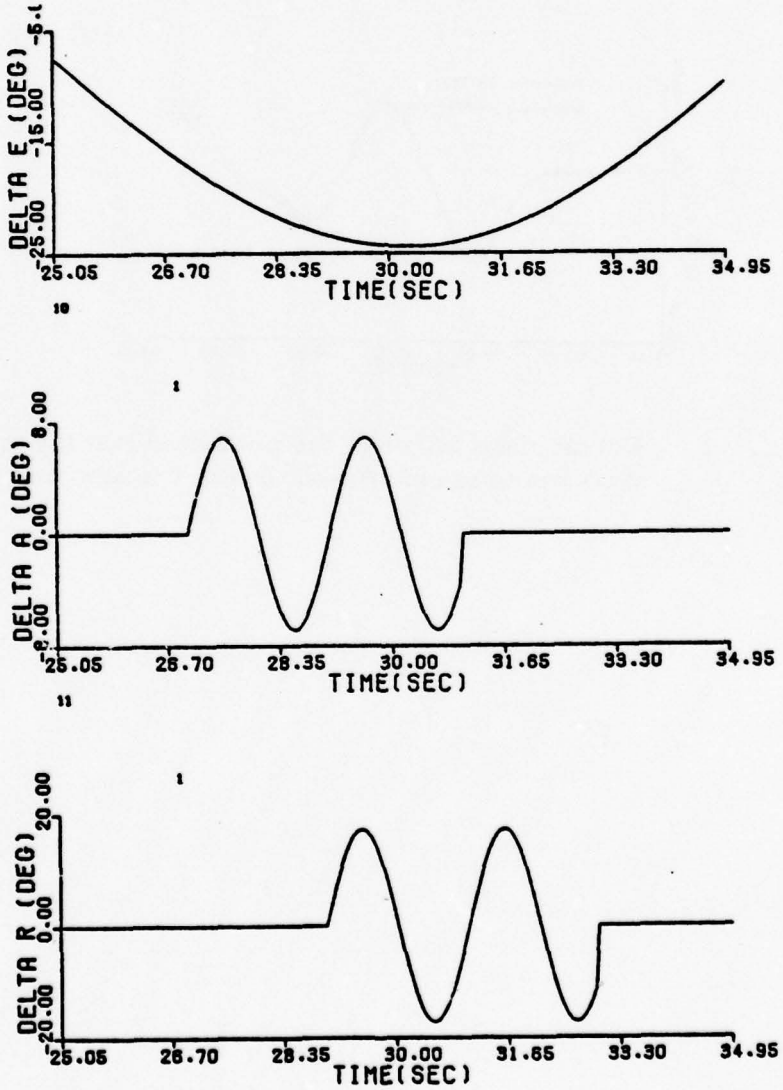

Figure 2.5-2 The controls δ_e, δ_a and δ_r used in predicting a new maneuver

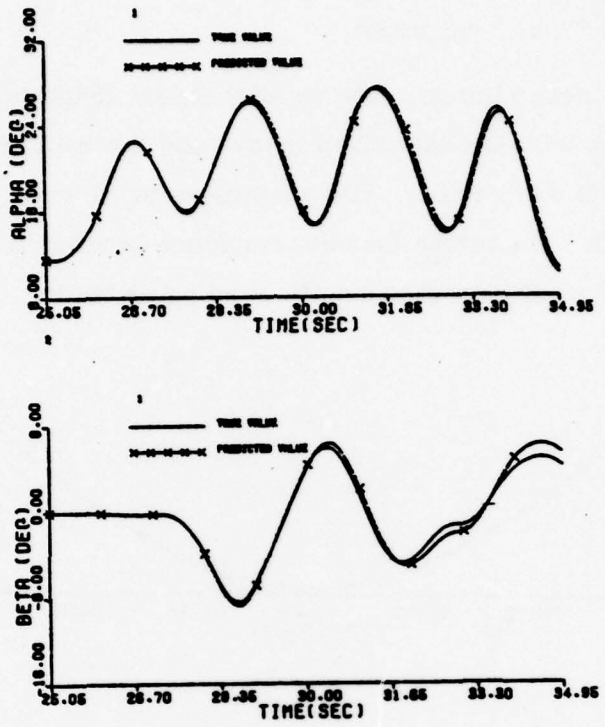

Figure 2.5-3 Comparison between the predicted and the true time histories of α and β for the new maneuver

3. SUMMARY OF ACTUAL FLIGHT TEST DATA RESULTS

3.1 FLIGHT TEST CONDITIONS AND DESCRIPTION OF MANEUVERS

The T-2C flight test data were gathered with gear up and speed brake retracted under the following conditions:

True Airspeed	-	75 to 150 meters/sec
Mach No.	-	0.25 to 0.4
Altitude	-	6000 to 7600 meters

The throttles were fixed during maneuvers. The Naval Air Development Center provided four sets of flight data consisting of eighteen maneuvers, amounting to over 600 seconds of 20 Hertz sampled data. The type of input used to generate each maneuver is described in the last column of Table 3.1-1. The first column gives the date of the flight set and the second column denotes the flight number and the maneuver number that goes with the input used.

The maneuvers F1M1, F4M9 and F6M1 have 360° rolls and the maneuver F4M10 has two 360° rolls. The angle of attack, α, ranges from -4° to 40° and the sideslip angle, β, covers the range from -14° to 26°. Most of the maneuvers have a trim α between 10.5° and 11.5° and a trim V (i.e., true airspeed) between 90.0 and 95.0 meters/sec. The maneuvers F4M7 and F4M8 have a trim α between 5.5° and 6.5° and a trim V between 115 and 120 meters/sec.

3.2 ESTIMATION RESULTS - FIRST STEP OF THE EBM METHOD

The extended Kalman-Bucy filter/Bryson-Frazier smoother as discussed in Volume II was used to process the eighteen maneuvers F1M1, F2M1, ..., F6M1 to obtain the estimation results of this study. Bias states and scale factor states were added to the filter/smoother

Table 3.1-1 Description of the Actual T-2C Data Processed with the EBM System Identification Method

Date of Flight	Flight No. and Maneuver No.	Approximate Duration of Maneuver (sec.)	Type of Input
Nov. 5, 1975	F1M1	16	Aft Stick, full rudder pedal (360° roll)
Dec. 10, 1975	F2M1	34	Random fore & aft stick
	F2M2	35	Random side to side lateral stick
	F2M3	40	Sequential doublets - δ_e, δ_a, δ_r
Dec. 29, 1975	F3M1	34	*Longitudinal Doublet*
	F3M2	25	Random Side to Side Rudder Input
	F3M3	39	Sequential Random - δ_e, δ_a, δ_r ($\beta_o = 0^o$)
Aug. 26, 1976	F4M1	21	Longitudinal Stick ramp plus sine wave
	F4M2	75	Sequential Random - δ_e, δ_a, δ_r ($\beta_o = -5^o$)
	F4M3	46	Sequential Random - δ_e, δ_a, δ_r ($\beta_o = 5^o$)
	F4M4	30	Full aft Stick plus pulses (spin)
	F4M5	60	Longitudinal Limit Cycle
	F4M6	38	Shallow Bank to Stall
	F4M7	40	Steep Bank to Stall (360° roll)
	F4M8	29	Pull-up from Dive (360° roll)
	F4M9	29	Coordinated Control Spin Entry (360° roll)
	F4M10	28	Coordinated Control Spin Entry (2-360° rolls)
Nov. 5, 1975	F6M1	17	Aft Stick, full Lateral Stick

to handle the instrumentation biases and scale factors that are inherent in real data. The estimates of the scale factors and the biases are given in Tables 3.2-1 and 3.2-2. The last column of Table 3.2-2 lists the flight numbers for which estimated biases were observed. Note that no biases were observed for α and V for the maneuvers of Flight Number 4. We see from Table 3.1-1 that the maneuvers of Flight No. 4 were run on August 26, 1976 and that the other maneuvers were run before December 30, 1975. The roll rate and pitch rate biases have large magnitudes, and there was no consistency in the estimates of the sideslip angle bias. The measured variables are described in Table 3.2-3.

The estimated values of the states, forces and moments of F1M1 are compared with their corresponding measured values in Figures 3.2-1, 3.2-2 and 3.2-3. Comparisons of α and of β are given in Figure 3.2-1. Therein, the estimated values are plotted with crosses at one second intervals. Note how the estimator smooths out the measured seesaw values caused by the vibration of the noseboom. In Figure 3.2-2 observe how the estimator smooths through the loss of the airspeed measurement shortly before 8.0 seconds. The estimator smoothed out the high noise level on the yaw rate. The estimation results, of which those of F1M1 are typical, were very good for all states, forces and moments of all the maneuvers of the flights, with the exception of F4M10. In F4M10 the roll angle passes through 180° several times; the measurement of the roll angle is not a good measurement in the neighborhood of 180°.

Table 3.2-1 The estimated values of the scale factors of α and β.

Measured Variable	Estimated Scale Factor
α	.78
β	.805

Table 3.2-2 The estimated values of the biases of the measured variables

Measured Variable	Estimated Bias	Estimated in the Maneuvers of the Following Flights
α	2°	1, 2, 3 and 6
β	Variable up to 5°	all
V	-3.9 m/sec	1, 2, 3 and 6
p	-6.1°/sec	all
q	-2.7°/sec	all
δ_a	1.8°	all
Fore-Aft accel.	-0.6 m/sec^2	all
Normal accel. (c.g.)	-1.6 m/sec^2	all
Normal accel. (off c.g.)	1.0 m/sec^2	all
Lateral accel. (c.g.)	-.13 m/sec^2	all
Rate gyro alignment	-3°	all

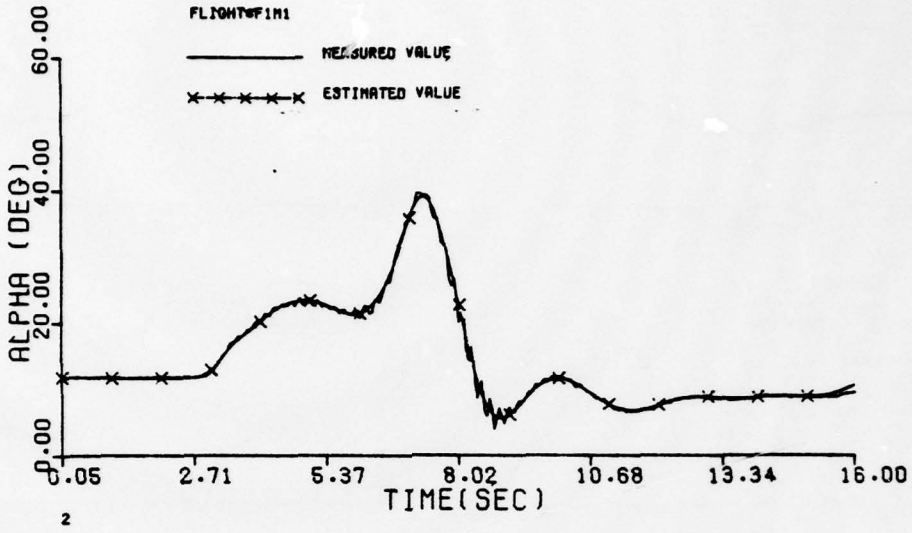

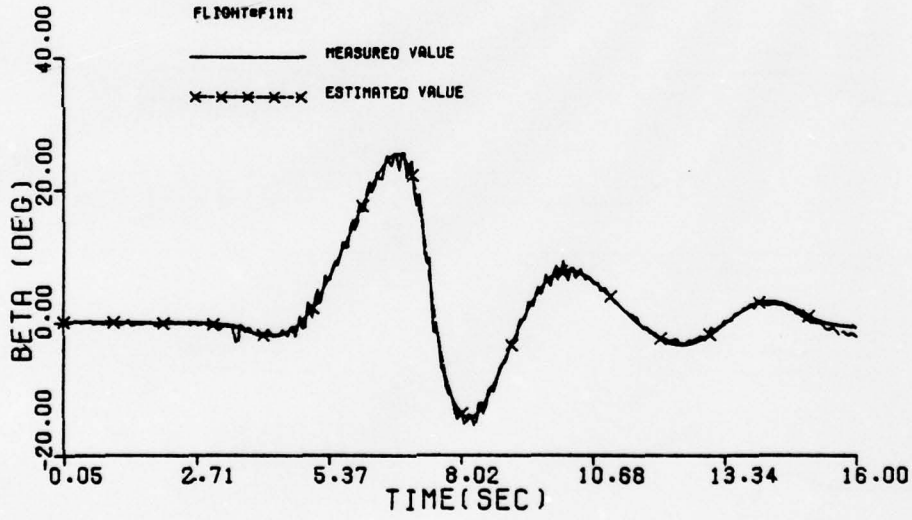

Figure 3.2-1 Comparison between the measured and the estimated values of F1M1 for α and β

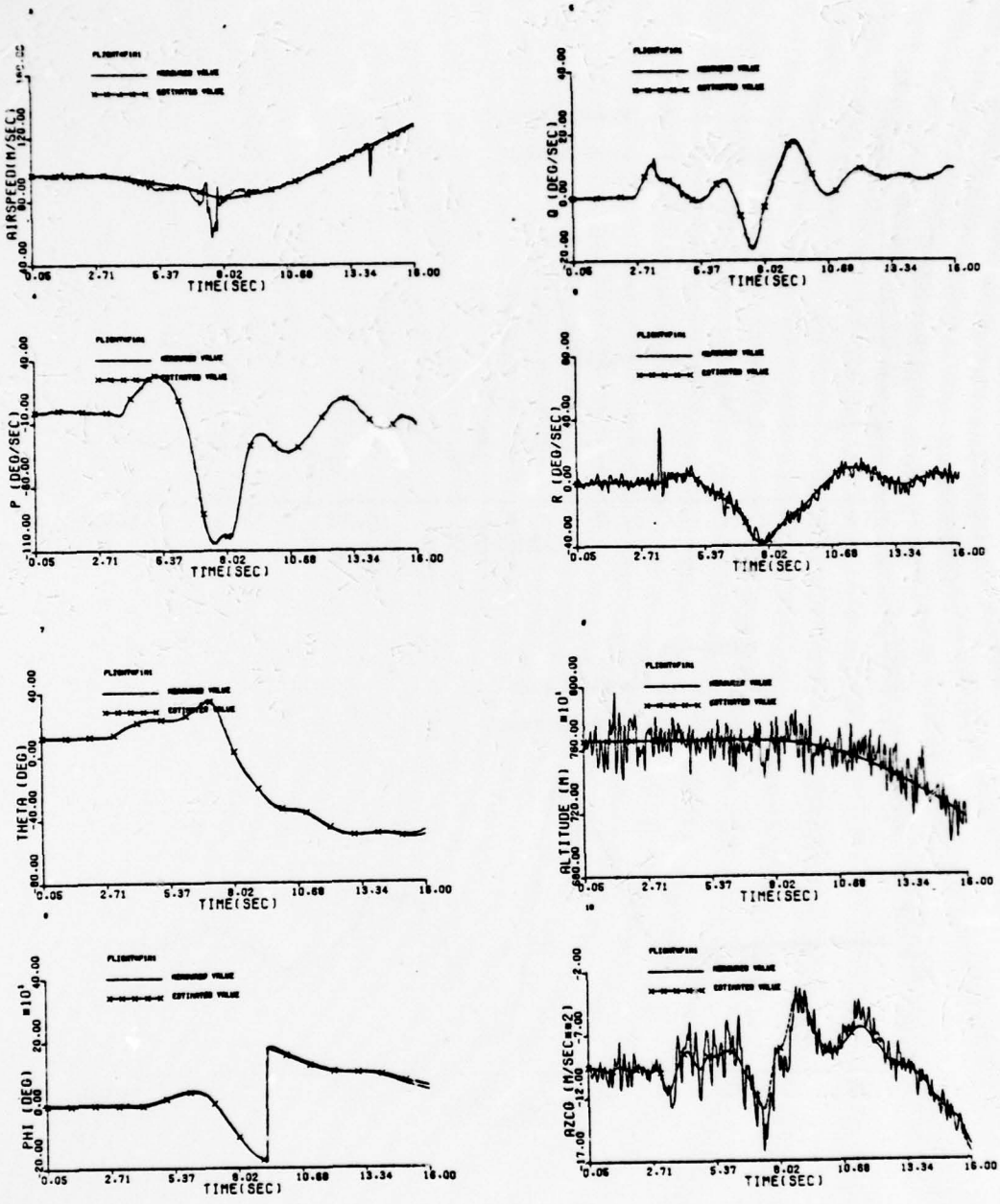

Figure 3.2-2 Comparison between the measured and the estimated values of F1M1 for V, p, q, r, θ, ϕ, z and AZCG

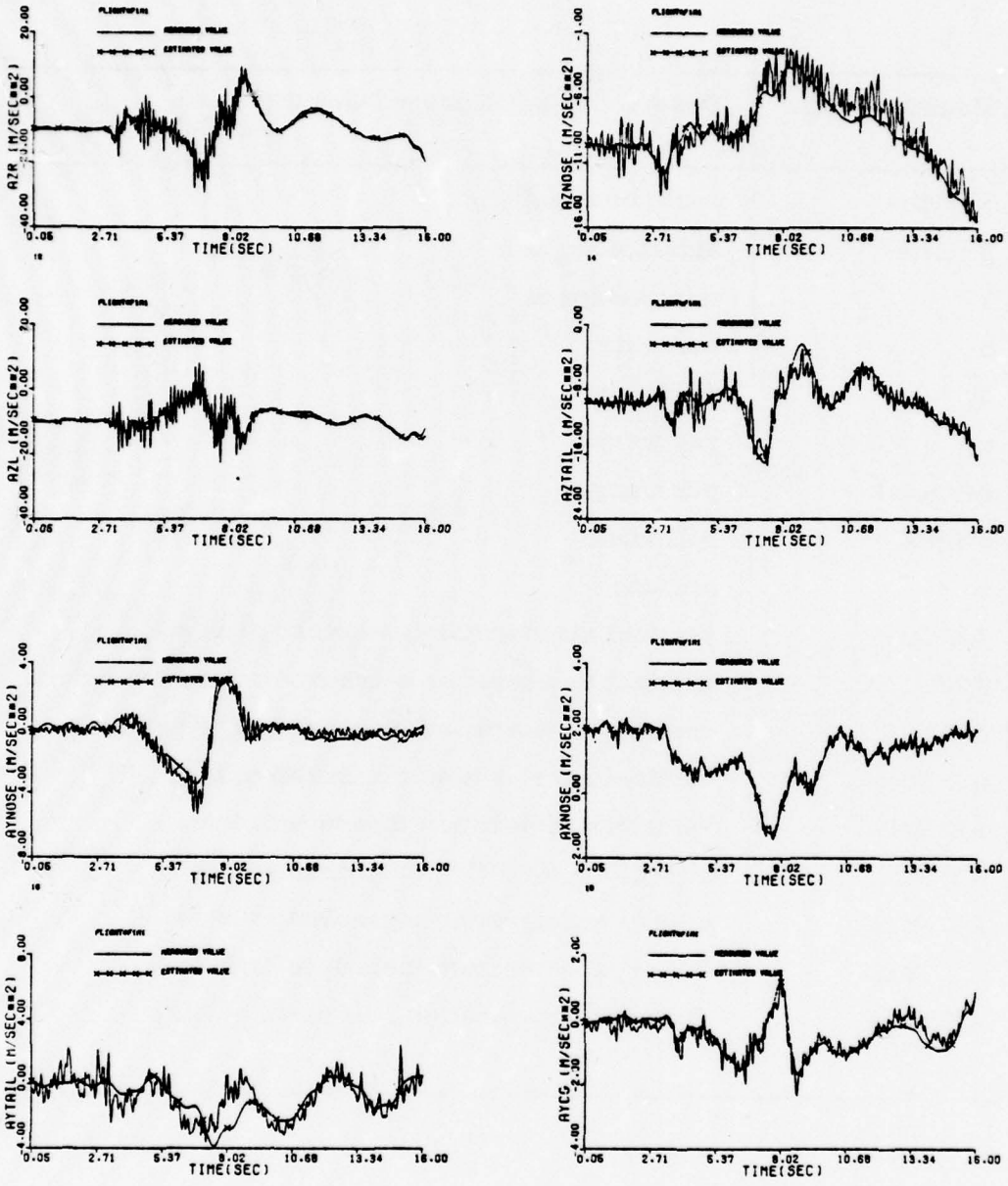

Figure 3.2-3 Comparison Between the Measured and the Estimated Values of F1M1 for the Accelerations

Table 3.2-3 List of the measured variables of the T-2C actual flight test data

Measured Qty.	Description of Measured Quantity
α (alpha)	angle of attack
β (Beta)	sideslip angle
V	total airspeed
p	roll rate
q	pitch rate
r	yaw rate
θ(Theta)	pitch angle
ϕ (Phi)	roll angle
z	attitude
AZ CG	vertical acceleration measured at c.g.
AZR	vertical acceleration measured at right wing
AZL	vertical acceleration measured at left wing
AZ Nose	vertical acceleration measured at nose
AZ Tail	vertical acceleration measured at tail
AY CG	lateral acceleration measured at c.g.
AY Nose	lateral acceleration measured at nose
AY Tail	lateral acceleration measured at tail
AX Nose	Fore-aft acceleration measured at nose

3.3 SUMMARY OF THE LATERAL MODEL IDENTIFICATION RESULTS - SECOND STEP OF THE EBM METHOD

The states α and β were used for defining the subspaces for modeling. The subspaces in α were created by partitioning α at one degree intervals between -4° and 25° and at five degree intervals between 25° and 40°. The subspaces in β were handled by using spline functions with knots at five degree intervals.

The estimated results of the eighteen maneuvers F1M1, ..., F6M1 were processed by the stepwise multiple linear regression (SMLR) technique, the modeling phase of the EBM system identification method. Nonlinear models of the lateral coefficients C_y, C_ℓ and C_n were identified as functions of the variables α, β, p, r, δ_a and δ_r. Table 3.3-1 contains a listing of the identified derivatives, where the limit $\beta\max(\alpha)$ is the maximum value achieved by the sideslip angle β over the eighteen maneuvers at the angle of attack α.

Table 3.3-1 The derivatives of the lateral coefficients that were identified with nonlinear models, $-4 \le \alpha \le 40^\circ$, $0^\circ \le |\beta| \le \beta\max(\alpha)$

C_y derivatives	C_ℓ derivatives	C_n derivatives
$C_{y_\beta}(\alpha, \beta)$	$C_{\ell_\beta}(\alpha, \beta)$	$C_{n_\beta}(\alpha, \beta)$
-	$C_{\ell_{\delta_a}}(\alpha)$	$C_{n_{\delta_a}}(\alpha)$
$C_{y_{\delta_r}}(\alpha)$	$C_{\ell_{\delta_r}}(\alpha)$	$C_{n_{\delta_r}}(\alpha)$
-	$C_{\ell_p}(\alpha)$	$C_{n_p}(\alpha)$
-	$C_{\ell_r}(\alpha)$	$C_{n_r}(\alpha)$

The SMLR technique found the derivatives with respect to $\dot{\beta}$ to be statistically insignificant. The derivatives $C_{y_p}(\alpha)$ and $C_{y_r}(\alpha)$ were masked by the excessively high measurement noise level on the yaw rate measurement. For in the sideslip equation of motion the yaw rate multiplies the total airspeed whose product presents a high noise level in the identification of the C_y derivatives.

The identified state and control derivatives were compared with the wind tunnel model and the dynamic derivatives were compared with the theoretical prediction models of Bihrle Applied Research. Typical examples of these comparisons are given in what follows.

The comparison of the $C_{y_\beta}(\alpha, \beta)$, $-4^\circ \leq \alpha \leq 40^\circ$, $\beta = 9^\circ$ is shown in Figure 3.3-1a. The curves match well between $\alpha = 6^\circ$ and $\alpha = 35^\circ$. Outside of this α range where there was sparse data, the identified model is still reasonably good. This is a typical example of the good match between the identified model of C_y and the wind tunnel data.

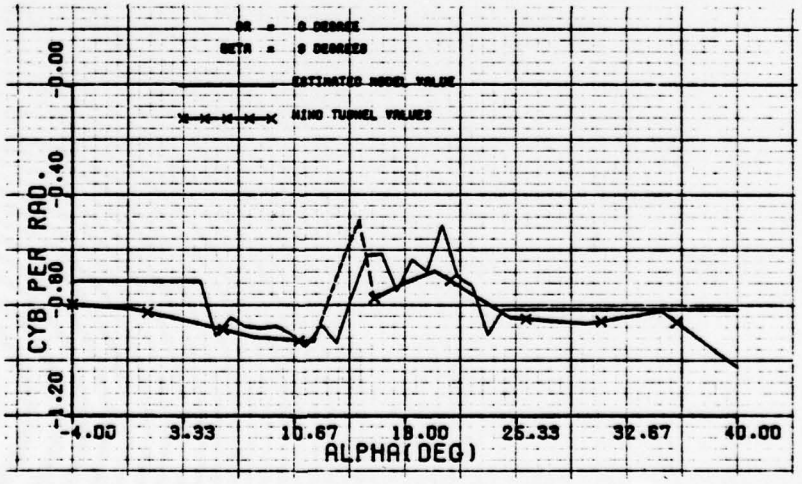

Figure 3.3-1a Comparison between the $C_{y_\beta}(\alpha, \beta)$ identified model and the wind tunnel model for $\beta = 9^\circ$.

This same derivative is also shown in Figure 3.3-1b for the range $0 \leq |\beta| \leq 10^{o}$, $\alpha = 22.5^{o}$; the EBM technique identified the "deep well".

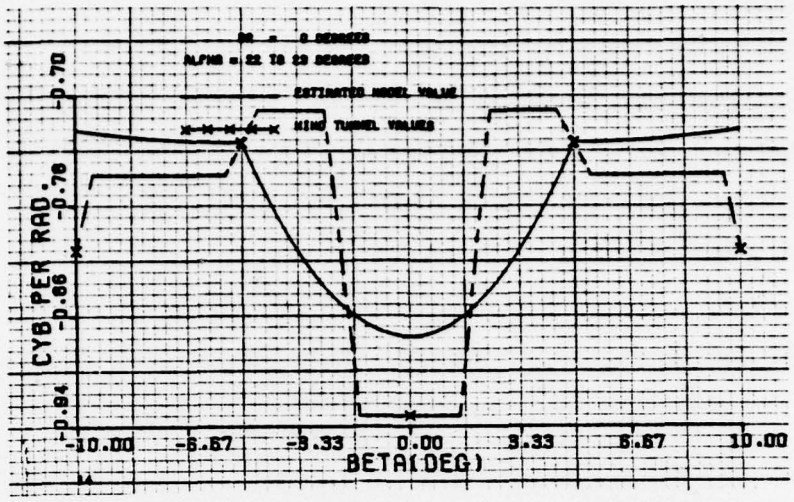

Figure 3.3-1b Comparison between the identified model and the wind tunnel data of $C_{y_\beta}(\alpha, \beta)$ at $\alpha = 22.5^{o}$.

The identified model of $C_{\ell_{\delta_a}}(\alpha)$ is given in Figure 3.3-2. It compares well with the wind tunnel data at α below stall, and its drop in controllability above stall coincides with that of the wind tunnel data. For α between 18 and 26, the identified model has slightly smaller magnitude than the wind tunnel, but they coincide above an α of of 30 .

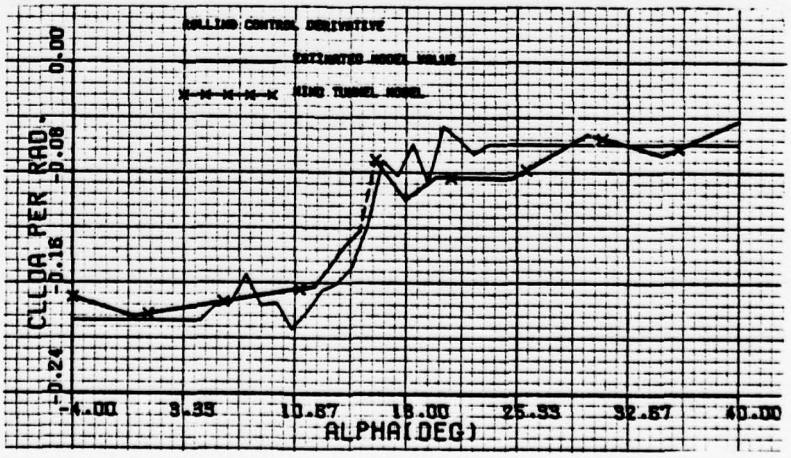

Figure 3.3-2 Comparison between the identified model and the T-2C wind tunnel data for $C_{\ell_{\delta_a}}$

The identified model of the dynamic derivative $C_{\ell_p}(\alpha)$ is presented in Figure 3.3-3. At low α the identified model has smaller values than the theoretical prediction model. The two curves cross near stall and the identified model hovers about the zero axis between 16° and 20° whereas the theoretical prediction goes positive and reaches a peak of 0.30 per rad. The two curves are close for α above 20°.

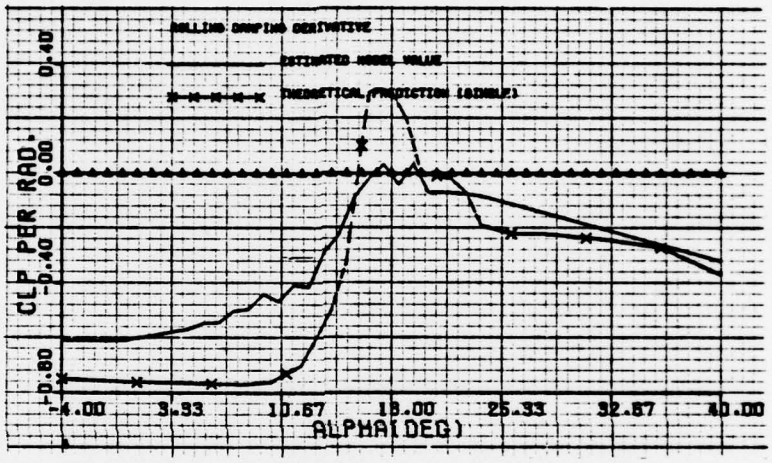

Figure 3.3-3 Comparison between the C_{ℓ_p} identified model and the theoretical prediction model of Bihrle Applied Research

The identified model of the dynamic derivative $C_{\ell_r}(\alpha)$ is plotted in Figure 3.3-4. It has a slightly steeper slope at low α and drops off more sharply at stall than the theoretical prediction model. Above $\alpha = 18°$ the identified model lies slightly under the theoretical prediction.

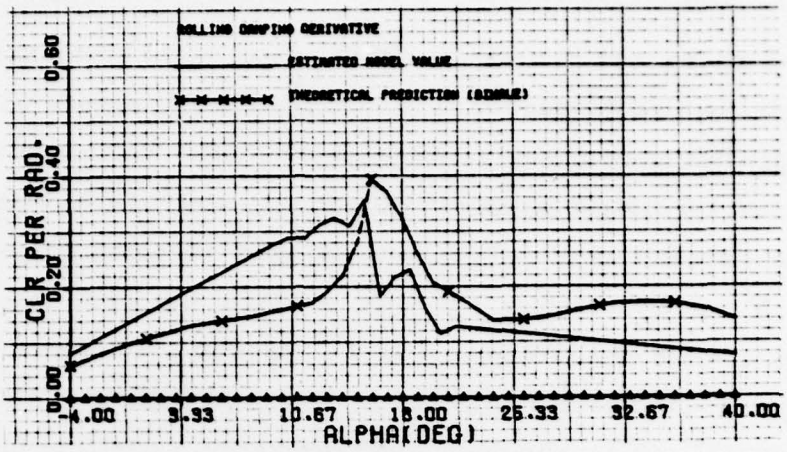

Figure 3.3-4 Comparison between the C_{ℓ_r} identified model and the theoretical prediction model of Bihrle Applied Research

The identified model of C_{n_β} (α, β) for $\beta = 9°$ is given in Figure 3.3-5. The identified model closely matches the wind tunnel data at low α, where it is nearly a constant value. At stall the identified model drops off with the wind tunnel value where they take on some negative values. The two curves have close agreement above $\alpha = 18°$.

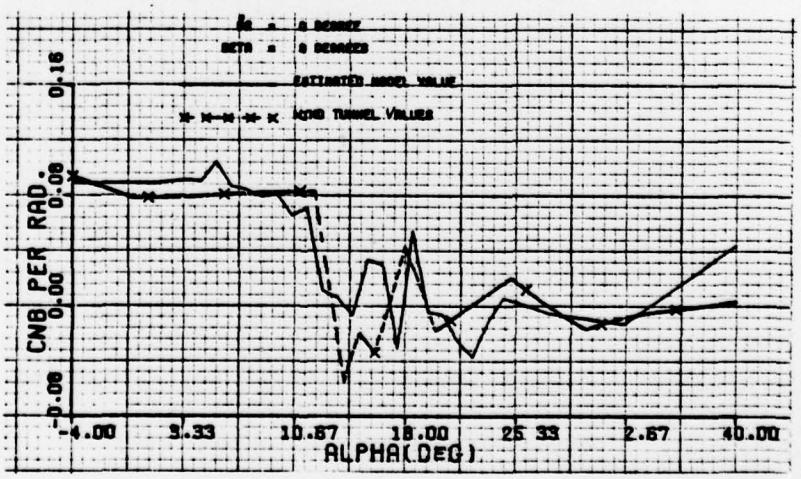

Figure 3.3-5 Comparison between the identified model and the T-2C wind tunnel data for C_{n_β} for $\beta = 9°$

The identified dynamic derivative $C_{n_p}(\alpha)$ is plotted in Figure 3.3-6 where it is compared with the theoretical prediction model of Bihrle Applied Research. The identified model agrees with the theoretical prediction at angles of attack below stall. The identified model reaches its highest positive value of .113 at $\alpha = 16.5°$ whereas the theoretical prediction model continues to grow reaching its peak of 0.365 at $\alpha = 18°$. After reaching a peak at $\alpha = 16.5°$ the identified model drops off to a value of -.076 at $\alpha = 20.5°$, rises to .048 at $\alpha = 22.5$; and drops to -.051 at $\alpha = 23.5$ before leveling off about -.075 over the α range [25°, 40°]. The theoretical prediction model, on the other hand, drops from its peak at $\alpha = 24°$, then rises to .195 at $\alpha = 30°$ before dropping to .06 at $\alpha = 38°$.

Of particular interest is the difference between these two models over the α range [20°, 35°]. In this range the theoretical prediction model has values greater than .10, while the identified model has values

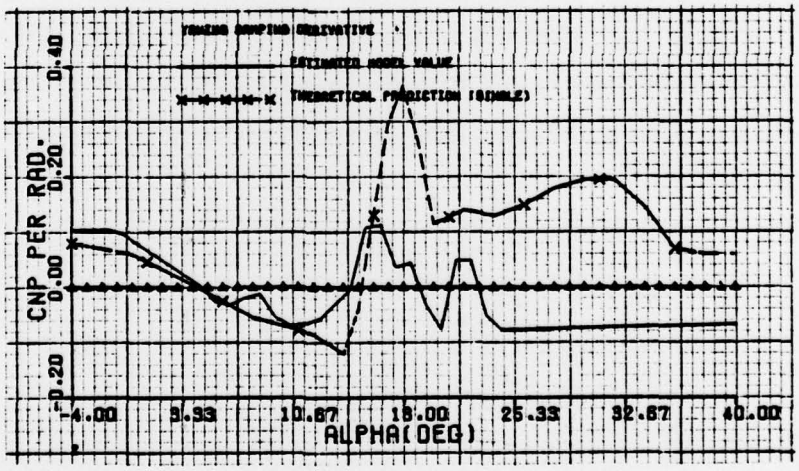

Figure 3.3-6 Comparison between the C_{n_p} identified model and the theoretical prediction model of Bihrle Applied Research

around -.075, except for the sharp rise and decline between $\alpha = 21^{\circ}$ and 23°. This difference is highly significant when correlated with the findings of the simulation study. Therein, the initial conditions and the recorded control time histories of the actual T-2C flight data were used to drive the synthetic T-2C model composed of the wind tunnel model and the theoretical prediction model of Bihrle Applied Research. The synthetic responses were drastically different from the actual flight data until a change in the theoretical prediction model of C_{n_p} was made. By trial and error a constant value of C_{n_p} = -.06 was found to give stability to the simulated data. Note that the identified model of C_{n_p} (about -.075) obtained by processing the actual T-2C flight data agrees with the modification of C_{n_p} obtained by trial and error in the simulation study. This result provides strong evidence that the Bihrle model for C_{n_p} is inaccurate.

The identified model of C_{n_r} (α) is plotted in Fugure 3.3-7. It is a good match to the theoretical prediction model of Bihrle Applied Research. Around stall there appears to be a difference between the curves of about 1° shift in α.

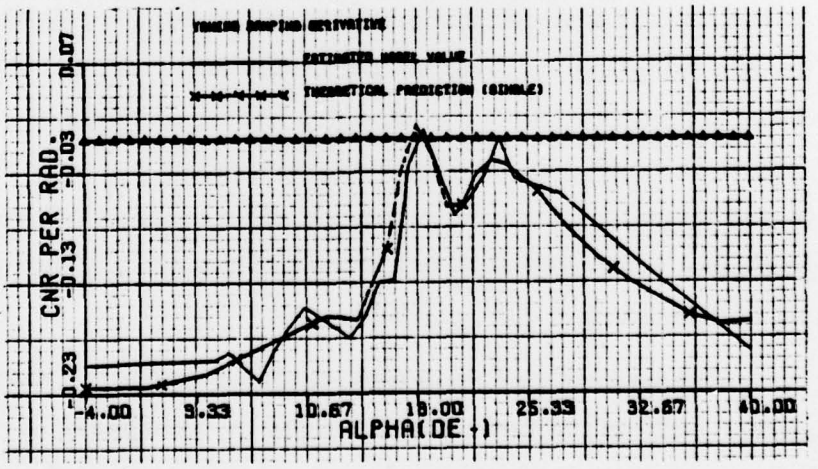

Figure 3.3-7 Comparison between the C_{n_r} identified model and the theoretical prediction model of Bihrle Applied Research

3.4 SUMMARY OF THE LONGITUDINAL MODEL IDENTIFICATION RESULTS - SECOND STEP OF THE EBM TECHNIQUE

The longitudinal coefficients C_x, C_z, and C_m are functions of the following variables:

α	-	angle of attack
β	-	sideslip angle
q	-	pitch rate
δ_e	-	elevator deflection
$\dot{\alpha}$	-	α rate

The states α, β and δ_e are used for defining the subspaces for modeling. Subspace modeling is conducted in two steps for the modeling of C_m. The first uses a partitioning of the α space [-4°, 40°] together with spline functions to handle the subspaces of the β and the δ_e space. The subspaces in α are generated by partitioning the α space into one degree intervals $[\alpha_i, \alpha_i + 1°]$, α_i = -4°, -3°, ... , 24° and five degrees intervals $[\alpha_i, \alpha_i + 5°]$, α_i = 25°, 30°, 35°. The eighteen estimation data files (i.e., one for each of the maneuvers F1M1, F2M1, ... , F4M10 and F6M1) generated by the estimation phase of the EBM system identification method are transformed into thirty-two new estimation data files for modeling by using the partitions on α and by collecting together the data from all eighteen maneuvers having an angle of attack within a given α-interval. In this first step the subspaces in β and δ_e are handled by using spline functions. Since a longitudinal coefficient is symmetric with respect to the sideslip angle, a quadratic spline function as a function of $|\beta|$ is used.

The second step uses a partitioning of the δ_e space [-28°, 2°] together with spline functions to handle the subspaces of α. The space of δ_e is partitioned into one degree intervals $[\delta_{e_i}, \delta_{e_i} + 1°]$, δ_{e_i} = -28°, -27°, ... , 1°. The eighteen estimation data files generated by

the estimation phase of the EBM method are transformed into thirty new estimation data files for modeling by using the partitions on δ_e and by collecting together the data from all eighteen maneuvers having an elevator control deflection within a given δ_e-interval. In this second step the subspaces in α are handled by using spline functions.

Nonlinear models of the C_m coefficient were identified for the following derivatives:

$C_{m_\alpha}(\alpha, \delta_e)$, $-28° \leq \delta_e \leq 1°$, $\alpha\,\mathrm{MIN}(\delta_e) \leq \alpha \leq \alpha\,\mathrm{MAX}(\delta_e)$

$C_{m_\beta}(\alpha, \beta)$, $-4° \leq \alpha \leq 40°$, $0 \leq |\beta| \leq \beta\,\mathrm{MAX}(\alpha)$

$C_{m_q}(\alpha)$, $-4° \leq \alpha \leq 40°$

$C_{m_{\dot\alpha}}(\alpha)$, $-4° \leq \alpha \leq 40°$

where $\alpha\,\mathrm{MIN}(\delta_e)$ is the minimum value of the angle of attack for all maneuvers at the elevator setting δ_e and, similarly, $\alpha\,\mathrm{MAX}(\delta_e)$ is the maximum value.

The identified dynamic derivative $C_{m_q}(\alpha)$ is compared with the theoretical prediction model of Bihrle Applied Research in Figure 3.4-1. The identified model of C_{m_q} varies between -11.4 and -8.0 at α below 4.5°. It then climbs slowly to its peak of 5.61 at $\alpha = 13.5°$ before falling to -7.7 at $\alpha = 18.5°$ where it levels off to values between -7.7 and -6.3 for α beyond 18.5°. The theoretical model holds almost level with a value of -10.3 below $\alpha = 14°$. It climbs sharply to a peak of 6.9 at $\alpha = 1.6°$ before dropping slowly to -4.5 at $\alpha = 30°$. The identified model has positive values for α between 11° and 16°, whereas the theoretical model has positive values for α between 15.5° and 22.5°.

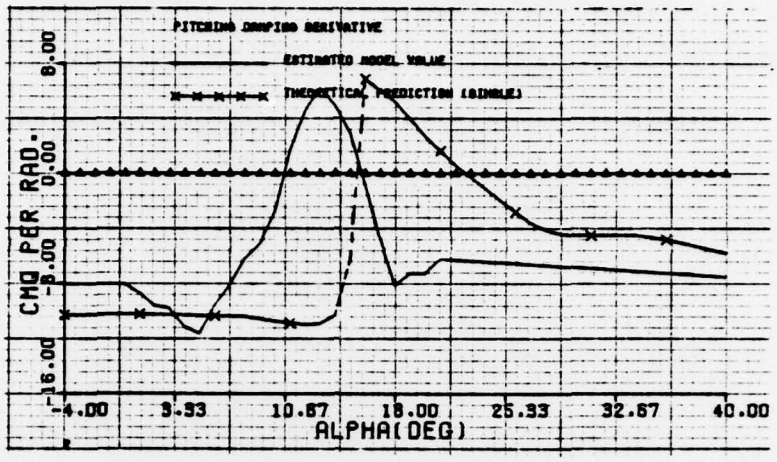

Figure 3.4-1 Comparison between the C_{m_q} identified model and the theoretical prediction of Bihrle Applied Research: Actual Flight Test Data

An example of the identified model of $C_{m_\alpha}(\alpha)$ at $\delta_e = -25.5°$ and its comparison with the wind tunnel is given in Figure 3.4-2.

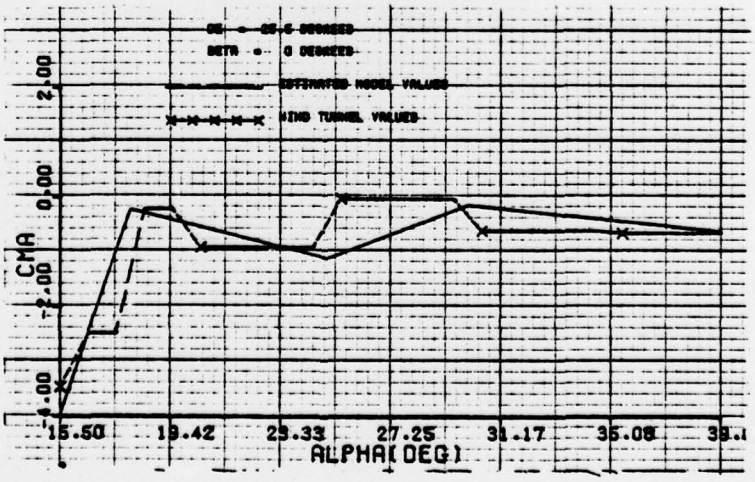

Figure 3.4-2 Comparison between the C_{m_α} identified model and the wind tunnel data for $\delta_e = -25.5°$: Actual Flight Test Data

The estimated values of $C_z(t)$ were compared with the wind tunnel values. The elevator control δ_e was used to subdivide the $C_z(t)$ estimates obtained from the eighteen maneuvers into data subsets. These subsets were ordered with respect to alpha and then plotted. The figures are contained in Volume III and they show a comparison with the wind tunnel data. The data in these subsets were never processed to generate an equation model of C_z, but the figures show that the model of the actual aircraft is close to that given by the wind tunnel analysis. In the figures, the real data values below stall almost coincide with the wind tunnel values which implies that the actual $C_{z_\alpha}(\alpha)$ is close to the wind tunnel data. Around stall there appears to be a hysteresis effect in the real data that is not accounted for by the wind tunnel model. For example, this can be observed in Figure 3.4-3 for $\delta_e = -14.5°$.

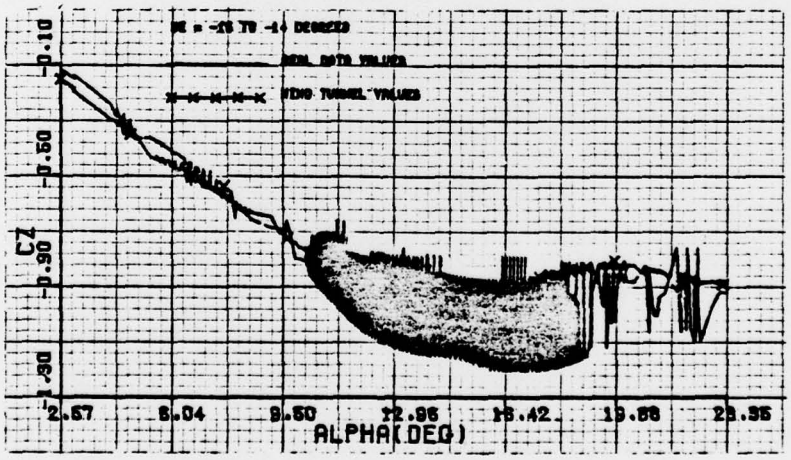

Figure 3.4-3 Comparison between the real data values and the wind tunnel data for C_z at $\delta_e = -14.5°$

The estimated values of $C_x(t)$ were compared with the wind tunnel values. In figures in Volume III the aerodynamic coefficient C_x is shown as a function of alpha for fixed one degree intervals of the elevator control. The range of the elevator control covers -28° to 0°. The figures were obtained as follows: A one-degree δ_e-interval was selected. All eighteen maneuvers were searched to find all $C_x(t)$ estimates having a corresponding δ_e within the selected δ_e-interval. The $C_x(t)$ estimates were then ordered according to alpha and plotted as a "real data values" curve in Volume III. The estimated states were used to evaluate the wind tunnel data in order to get a comparison. These curves have a dependency on β, q and $\dot{\alpha}$ built into them by the nature of the maneuvers. The curves exhibit some differences between the wind tunnel data and the actual aircraft. A hysteresis effect can be observed in the figures. The real data values are above the wind tunnel values at low alpha and at high alpha. Near stall they are below the wind tunnel values. For example, this can be observed in Figure 3.4-4.

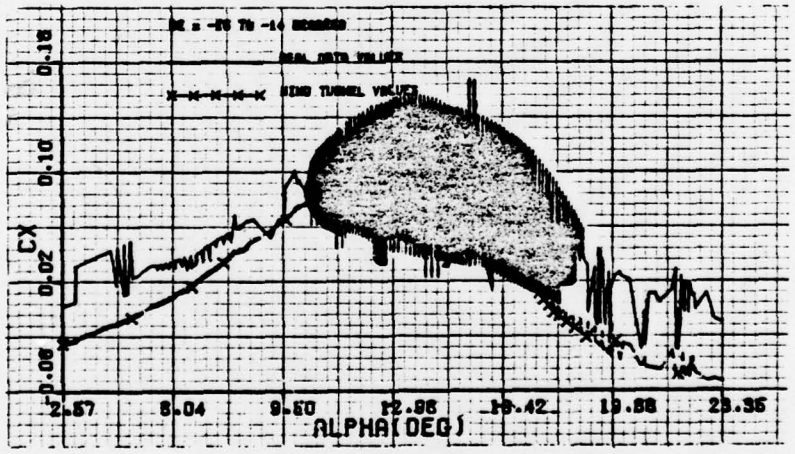

Figure 3.4-4 Comparison between the real data values and the wind tunnel for C_x at $\delta_e = -14.5°$

4. CONCLUSIONS AND RECOMMENDATIONS

4.1 CONCLUSIONS OF THE SIMULATION STUDY

The EBM methodology has been validated under controlled but realistic simulated conditions. The T-2C wind tunnel data and a theoretical prediction model of the dynamic derivatives were used to generate synthetic data. The controls, initial conditions, masses and thrusts of sixteen actual T-2C flight test data records were used to excite the T-2C wind tunnel data model to generate the sixteen synthetic maneuvers. The synthetic data were corrupted with realistic measurement noise levels and then processed with an extended Kalman-Bucy/Bryson-Frazier smoother to produce excellent estimated values of the states and of the forces and moments. Subspace modeling together with a step-wise multiple linear regression technique were used to identify a global state/control dependent model of the force and moment coefficients. The identified model agrees well with the T-2C wind tunnel data. The high nonlinearities were accurately identified. The identified global model gave excellent predicted responses for a new maneuver not used in the identification process.

4.2 CONCLUSIONS OF THE REAL DATA ANALYSIS

The EBM methodology was successfully tested on flight test data and provided good aerodynamic models of the T-2C aircraft.

Within the first step of the EBM method, the data from eighteen maneuvers which had been collected over a period of ten months were processed, and large biases were accurately estimated in angle of attack, sideslip angle, total airspeed, roll rate, pitch rate, fore-aft acceleration, normal acceleration and rate gyro alignment. The method satisfactorily handled the high noise levels on the yaw rate, the rudder deflection, the total airspeed, the acceleration measurements (as well as the losses of some measurements

over extended intervals of flight), and the nose boom vibration present in the angle of attack and sideslip angle measurements. The estimation results which are documented in Volume III and exemplified in Section 3.2 demonstrate that the first step of the EBM method performed well on the T-2C flight test data.

Within the second step of the EBM method detailed detailed nonlinear models of the aerodynamic derivatives were identified and compared with the wind tunnel data. . Most of the identified state and control derivatives matched well with the wind tunnel data. The identified dynamic derivatives were compared with the theoretical prediction models of Bihrle Applied Research. The identified models of C_{ℓ_p} and C_{ℓ_r} agreed fairly well with the theoretical prediction models with the exception that the identified model hovers about a zero value around stall while the theoretical model shows positive values. The identified model of C_{ℓ_r} drops off more sharply after stall than the theoretical model. The identified C_{n_r} compares well for all alpha, but C_{n_p} only matches at low alpha. At high alpha, C_{n_p} is predicted to have values above .10 but the identified model showed that the values are around -.075. The simulation study documented in Volume II found that the theoretical prediction of C_{n_p} is inaccurate at high α and that a constant value of -.06 provided a better model for generating synthetic responses which mimic more closely the real data. The identified model of C_{n_p} obtained by processing the actual T-2C flight data agrees with the modification of the theoretical model of C_{n_p} obtained by trial and error in the simulation study.

The modeling results of the real data analysis study demonstrate that the EBM system identification method provides accurate nonlinear modeling of high α/β aerodynamic stability and control characteristics from flight test data.

4.3 MAJOR CONCLUSIONS OF THE STUDY

The major conclusions of this study are summarized as:

- Validated System Identification Tool

  The EBM methodology has been validated in great detail on both synthetic and actual flight test data and has been shown to produce accurate nonlinear models. The EBM technique has been shown to be a practical tool for the modeling and analysis of vehicles aerodynamics that works on test data gathered under actual flight conditions.

- Advantage of Subspace Modeling

  Subspace modeling is an inherent feature of the EBM technique which circumvents the problem of identifying in one step complex nonlinear models over the entire α, βparameter region covered by the flight test. Instead, the problem is reduced to an easier procedure of identifying lower order models within the subspaces and then synthesizing a global model from these subspace models. In addition, breaking the modeling into subspaces provides a means of determining how much data is available in each subspace, and this in turn, provides a measure of model accuracy and confidence and provides an approach for determing when further flight testing is required to fill sparse subspaces.

- Data Versus Modeling Problems

  The two steps of the EBM technique, estimation in the time domain followed by modeling in the state domain, were established specifically to enhance the

process of distinguishing data problems from modeling problems. Data problems, if they exist, are uncovered in the estimation phase. That this works is exemplified by the results obtained by the application of the EBM technique to the actual T-2C data: measurement and axis alignment biases, scale factors, etc.

4.4 RECOMMENDATIONS

We recommend the following for improving future flight test data for system identification studies.

I. Instrumentation

A. Measure the Euler yaw angle ψ. This will permit better accuracy in estimating the bias on the yaw rate r.

B. Use sensors that measure the absolute values of the Euler pitch and bank angles, θ and ϕ, rather than measurements that are relative to arbitrary initial settings. This will allow the use of all maneuvers to estimate the biases of θ and ϕ, and it will provide a check on the condition $\theta = \alpha$ at trim.

C. Measure critical engine parameters for estimating thrust of engines. This will permit using the actual values of a varying thrust to identify a better drag model.

D. Use bank angle sensors that measure accurately through rolls greater than 180°. This will permit better estimation results at these bank angles during high roll rates and it will provide continuity through $\phi = 180°$.

E. Measure reliably the angular acceleration rates $\dot{p}$, $\dot{q}$ and $\dot{r}$. This will provide a check on off-c.g. acceleration measurements and more accurate estimation of $C_\ell(t)$, $C_m(t)$ and $C_n(t)$.

F. Use nose boom with less vibrational characteristics than that on the T-2C. This will provide better α and β data for estimation and modeling.

G. Use airspeed sensors which do not give a loss of measurements over extended intervals of flight. This permits better estimation and modeling results.

H. Use single channels for all measured variables. This provides the best signal-to-noise ratio for a measured quantity as compared to using a commutator.

I. Use pulse coded modulation (PCM) rather than pulse amplitude modulation (PAM). This will provide cleaner signals.

II. Rigorous Calibration and Consistency Checkout

A. Calibrate instrumentation using static data gathered in hangar (i.e., with aircraft in hangar, isolated from wind, turn instrumentation power on and record 100 seconds of data). This will permit the isolation and removal of unnecessary biases in linear and angular accelerations, in p, q and r, and in θ and ϕ.

B. Calibrate instrumentation using dynamic data gathered on a long runway (i.e., record data with aircraft jetting down runway in takeoff phase). This will permit the isolation and removel of unnecessary biases in α and β.

C. Calibrate instrumentation using dynamic data gathered in trim flight for various trim values of sideslip angle and total airspeed. This will permit the isolation and removal of biases in the controls for equilibrium flight.

D. Check out the consistency of the measured variables using several representative maneuvers of flight data. Use the equations of motion to test for consistency. This will provide a checkout on scale factors and axis alignment as well as the compatibility of the measured variables.

E. Fly calibration maneuvers before and after each flight set of maneuvers.

III. Improve Design of Maneuvers for System Identification

A. Fly more maneuvers and vary the variables such as trim airspeed and sideslip angle.

B. Design the maneuvers so that a good amount of data is provided at high and low α and at high β extremes rather than a few isolated data points.

C. Start and end each maneuver with long trim times.

IV. Precise Calculation of Aircraft Constants

A. Compute the aircraft mass for the beginning and the end of each maneuver.

B. Compute the limits on the changes in the moments of inertia due to weight distribution changes such as fuel consumption during maneuvers.

C. Provide calculations on the location of the center of gravity with respect to the aerodynamic center for each maneuver.